$LiNbO_3$ thin film growth on (0001)-GaN

Peter J. Hansen
Materials Department, University of California, Santa Barbara, California 93106

Yutaka Terao
Fuji Electric Co., Ltd., Gate City Ohsaki East Tower, 1-11-2 Osaki, Shinagawa-ku, Tokyo 141-0032, Japan

Yuan Wu
Materials Department, University of California, Santa Barbara, California 93106

Robert A. York and Umesh K. Mishra
Electrical and Computer Engineering Department, University of California, Santa Barbara, California 93106

J. S. Speck
Materials Department, University of California, Santa Barbara, California 93106

(Received 20 September 2004; accepted 29 November 2004; published 5 January 2005)

$LiNbO_3$ thin films were grown by rf magnetron sputtering on (0001)-GaN templates and AlGaN/GaN structures. The films were characterized by four-circle x-ray diffraction, atomic force microscopy (AFM), and transmission electron microscopy (TEM). No second phases, such as a Li-excess or Li-deficient phase, were detected by θ-2θ scans and the films were highly (0001) textured. $LiNbO_3$ $\{20\bar{2}4\}$ φ-scans and the electron diffraction pattern show that the films were epitaxially grown on GaN with crystallographic registry. The $LiNbO_3$ *c*-plane was parallel to the *c*-plane of the GaN, but there was a 30° in-plane rotation between the $LiNbO_3$ and GaN so that $[1\bar{1}00]_{LiNbO_3} \| [11\bar{2}0]_{GaN(AlGaN)}$ and the $LiNbO_3$ films had two variants of grains rotated 60° in-plane to each other. It was confirmed by high resolution TEM that there was a transition layer between $LiNbO_3$ and GaN. The films were annealed to improve the crystallinity and following annealing investigated using convergent beam electron diffraction (CBED) to determine the polarity. The films grow with a spontaneous polarization vector opposite to that of the underlying GaN film. © *2005 American Vacuum Society.* [DOI: 10.1116/1.1850106]

I. INTRODUCTION

Lithium niobate ($LiNbO_3$) has long been investigated because of its large pyroelectric, piezoelectric, electro-optic, and photoelastic coefficients,[1] and $LiNbO_3$ thin films have been extensively studied over the last decade. Most of the studies on $LiNbO_3$ have been driven by optical applications such as waveguides and second harmonic generation (SHG) or surface acoustic wave (SAW) filters. The utilization of the polar nature of $LiNbO_3$ has also been explored in electronic devices with the application of $LiNbO_3$ as a gate dielectric to form metal-ferroelectric-semiconductor (MFS) structures on silicon.[2,3]

GaN has recently been established as the enabling material for green, blue, and ultraviolet optoelectronics. GaN is also an enabling material for high-temperature, high power electronic applications due to its wide band gap, high electron saturation velocity, and high breakdown voltage. The ability of the AlGaN/GaN heterojuction to form a two-dimensional electron gas (2DEG) with a sheet carrier concentration of $\sim 1 \times 10^{13}$ cm^{-2} and mobilities of ~ 1500 cm^2 V^{-1} s^{-1} has resulted in the development of heterostructure field effect transistors structures for application in future generation microwave power devices[4–6]

The extremely high charge density at the AlGaN/GaN interface is the result of polarization effects in the *c*-oriented AlGaN/GaN system (in the wurtzite structure), and has been previously detailed.[7,8] The total polarization-induced charge density σ in an AlGaN/GaN structure is the sum of the polarization in the AlGaN, $\mathbf{P}$(AlGaN), and the polarization in the GaN, $\mathbf{P}$(GaN),

$$\sigma = P(\mathrm{AlGaN}) - P(\mathrm{GaN}).$$

In the absence of an electric field, the total polarization in wurtzitic AlGaN/GaN structures grown in the (0001) direction consists of piezoelectric (strain induced) polarization $\mathbf{P}_{PE}$ and the spontaneous polarization $\mathbf{P}_{SP}$ of the individual GaN and AlGaN layers. A 2.4% lattice mismatch at 300 K between AlN and GaN leads to piezoelectric polarization due to strain at the AlGaN/GaN interface. The direction of the piezoelectric field is from the cation-terminated (0001) face to the anion-terminated $(000\bar{1})$ face, and the field is given by

$$P_{PE} = 2\frac{a(x) - a(0)}{a(0)}\left[e_{31}(x) - e_{33}(x)\frac{C_{13}(x)}{C_{33}(x)}\right],$$

where $a(x)$ and $a(0)$ are the $Al_xGa_{1-x}N$ and GaN lattice constants, respectively, e_{31} and e_{33} are piezoelectric constants, and C_{13} and C_{33} are elastic constants. For cation-terminated (as is typically the case for MOCVD-grown) AlN and GaN layers, the spontaneous polarization is negative, or opposite to that of the growth direction for layers grown in the (0001)

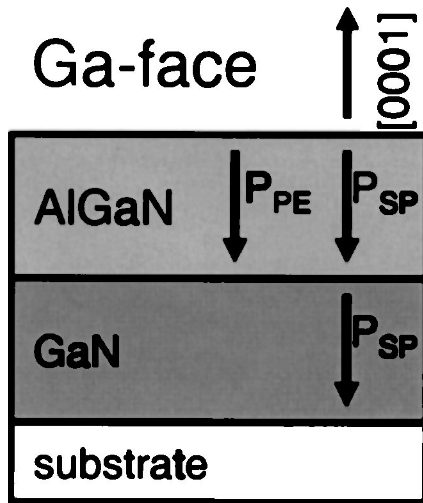

FIG. 1. Schematic of the AlGaN/GaN structure and polarization vector orientations for a MOCVD-grown (i.e., Ga-terminated) film.

direction. The spontaneous polarization increases in magnitude in going from GaN to AlN according to

$$P_{SP}(x) = (-0.052x - 0.029)\ \mathrm{C/m^2},$$

where x is the Al mole fraction in the $Al_xGa_{1-x}N$ layer. A schematic of the AlGaN/GaN system and the corresponding polarization vectors is shown in Fig. 1. The total polarization-induced charge density of these structures is given by

$$\sigma = P_{SP}(\mathrm{AlGaN}) + P_{PE}(\mathrm{AlGaN}) - P(\mathrm{GaN}).$$

The tremendous benefit of incorporating a ferroelectric with a high spontaneous polarization with semiconductor structures,[9] and particularly for the AlGaN/GaN system,[10,11] has recently been shown theoretically. Adding a ferroelectric material with a high spontaneous polarization to an AlGaN/GaN HEMT structure should result in an enhanced polarization-induced charge density and therefore an increased sheet charge in the 2DEG. $LiNbO_3$ is an excellent candidate for the polar material that could be incorporated with GaN HEMTs because of its high spontaneous polarization ($0.7-0.8\ \mathrm{C\,m^{-2}}$) (Ref. 12) and rhombehedral crystal structure that should match with the wurtzite crystal structure of GaN. The lattice parameters of the two materials are $a=5.147$ Å and $c=13.862$ Å for $LiNbO_3$ and $a=3.189$ Å, $c=5.185$ Å for GaN. This corresponds to a lattice mismatch of ~6.8% between $LiNbO_3$ and GaN with a 30° rotation of the $LiNbO_3$. Given a lattice mismatch this large, relaxed films can be expected. The discontinuity of the polarity at the $LiNbO_3$/GaN (AlGaN) interface and high spontaneous polarization of $LiNbO_3$ is expected to further enhance or reduce the charge at the AlGaN/GaN interface, depending on the polarization orientation of the $LiNbO_3$ film.

Recently the growth of GaN on $LiNbO_3$ substrates has been performed, with demonstration of polarity control of the GaN by controlling the polarity of the $LiNbO_3$.[13] In this article the growth of $LiNbO_3$ on GaN and AlGaN/GaN structures was performed to investigate the feasibility of incorporating $LiNbO_3$ as a polar material to induce additional charge at the AlGaN/GaN heterointerface.

II. EXPERIMENTAL PROCEDURE

A radio-frequency (rf) magnetron sputtering system was used to grow the $LiNbO_3$ films. The 3 in. diam commercially available $LiNbO_3$ sputtering target contained 5 mol % excess Li_2O. The substrates were positioned off-axis to the sputtering target and were rotated to ensure uniform heating and film thickness. The distance between the target center and the substrate was 4 in. 500 nm thick Ti films were evaporated on the backside of the $LiNbO_3$ and GaN/Al_2O_3 substrates for heat absorption during $LiNbO_3$ deposition.

To establish $LiNbO_3$ sputtering conditions, homoepitaxy on (0001)-$LiNbO_3$ single crystal substrates was first performed. Sputtering parameters such as gas mixture, gas pressure, substrate temperature, and rf power were varied in this optimization study. Once conditions were established for homoepitaxy, growth was performed on MOCVD-grown 2 μm thick (0001)-GaN templates as well as $Al_{0.33}Ga_{0.7}N$/GaN structures. Prior to $LiNbO_3$ deposition, the samples were cleaned using a standard degrease (acetone/isopropanol/deionized water) followed by a 30 s dip in HCl:DI 1:3 for 30 s.

The films were characterized by x-ray diffraction (XRD) using a Philips MRD Pro, and atomic force microscopy (AFM) images were obtained with a Digital Instruments 3100. Conventional transmission electron microscopy (TEM) studies were performed with a JEOL 2000FX. High-resolution images and convergent beam electron diffraction (CBED) patterns were obtained with a JEOL 2010HR. The polarity of the films was investigated using an $HF:HNO_3$ etch as well as convergent beam electron diffraction (CBED).

III. RESULTS AND DISCUSSION

It has been shown that for nonoptimized growth conditions, a Li-excess phase (Li_3NbO_4) or a Li-deficient phase ($LiNb_3O_8$) can be detected in the $LiNbO_3$ films by x-ray θ-2θ scans.[14] The (0006) $LiNbO_3$ x-ray diffraction peak is positioned at $2\theta\sim39°$, while the $(\bar{6}02)LiNb_3O_8$ peak is positioned at $2\theta\sim38°$ and (222) Li_3NbO_4 is positioned at $2\theta\sim37°$ in θ-2θ scans. During growth optimizations (homoepitaxial growth studies) both Li-rich and Li-deficient phases were observed. It was possible to eliminate the Li-deficient or Li-excess second phases by varying the sputtering conditions. No (0006) x-ray peak separation in the θ-2θ scans was observed for homoepitaxial films without a second phase peak. An example of each of these peaks is shown in Fig. 2. The full-width-at-half-maximum (FWHM) values of the rocking curve at the $LiNbO_3$ (0006) reflection and AFM images were compared to determine the optimized sputtering conditions. Outgrowths, of varied height and size, were observed in all of the homoepitaxial films by AFM and some films did not have a uniform surface morphology. The opti-

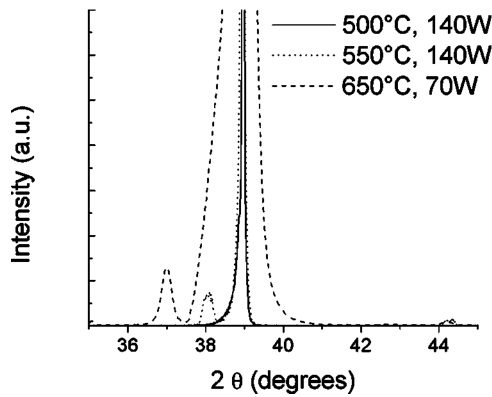

FIG. 2. θ-2 θ scans of $LiNbO_3$ homoepitaxial films showing Li deficient, Li rich, and optimized $LiNbO_3$ depositions.

mized conditions were chosen to yield a uniform film with a low rocking curve FWHM. The FWHM value of a homoepitaxial film grown under optimized conditions was $\Delta\omega = 0.00488°$, while a typical FWHM value of a single crystal substrate was $\Delta\omega = 0.00375°$. The optimized sputtering parameters obtained from these experiments were found to be 100 total sccm $Ar/O_2(Ar:O_2\ 60:40)$, chamber pressure 30 mTorr, rf power of 140 W, and substrate temperature of 500 °C. These conditions were then used to deposit $LiNbO_3$ films on GaN templates and AlGaN/GaN structures.

Figure 3(a) shows the θ-2θ x-ray diffraction (XRD) scan for the $LiNbO_3$ film on GaN. No second phase, such as Li_3NbO_4 or $LiNb_3O_8$, was evident from the scan. Only the $LiNbO_3$ (0006) peak was observed in the θ-2θ scan in addition to the GaN (0002) and Al_2O_3 (0006) at $2\theta = 34.8°$ and $2\theta = 41.7°$, respectively. The full width at half maximum (FWHM) of the rocking curve of the $LiNbO_3$ (0006) peak was 0.98°, as shown in Fig. 3(b). A θ-2θ scan of a $LiNbO_3/Al_{0.33}Ga_{0.67}N/GaN$ structure is shown in Fig. 3(c) and the corresponding $LiNbO_3$ (0006) rocking curve is shown in Fig. 3(d). No peaks indicating the presence of Li deficient or Li rich phases were observed in the θ-2θ scan of the $LiNbO_3$ film on AlGaN/GaN. Only peaks corresponding to GaN (0002), AlGaN (0002), $LiNbO_3$ (0006), and Al_2O_3 (0006) were observed. The rocking curve FWHM of the $LiNbO_3$/AlGaN sample was 1.38°. Given the ~6.8% lattice mismatch between $LiNbO_3$ and GaN (with a 30° rotation of the $LiNbO_3$) in the (0001) plane, a relatively high mosaic for the $LiNbO_3$ film is not surprising.

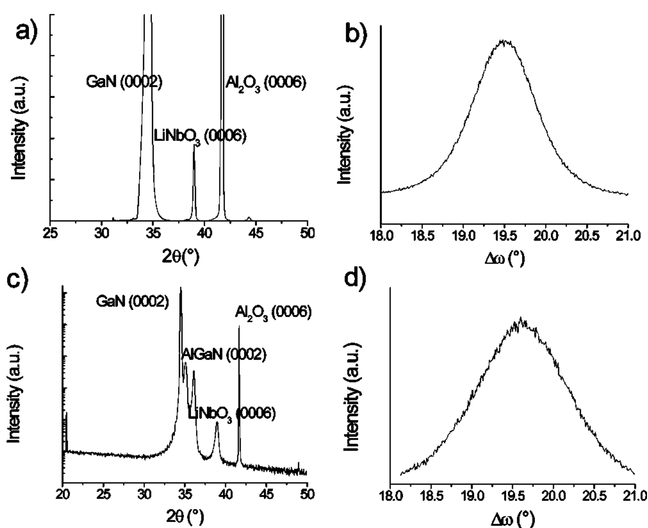

FIG. 3. θ-2θ scans of $LiNbO_3$/GaN (a) and $LiNbO_3$/AlGaN/GaN (c) and $LiNbO_3$ (0006) rocking curves of each respective sample (b) and (d).

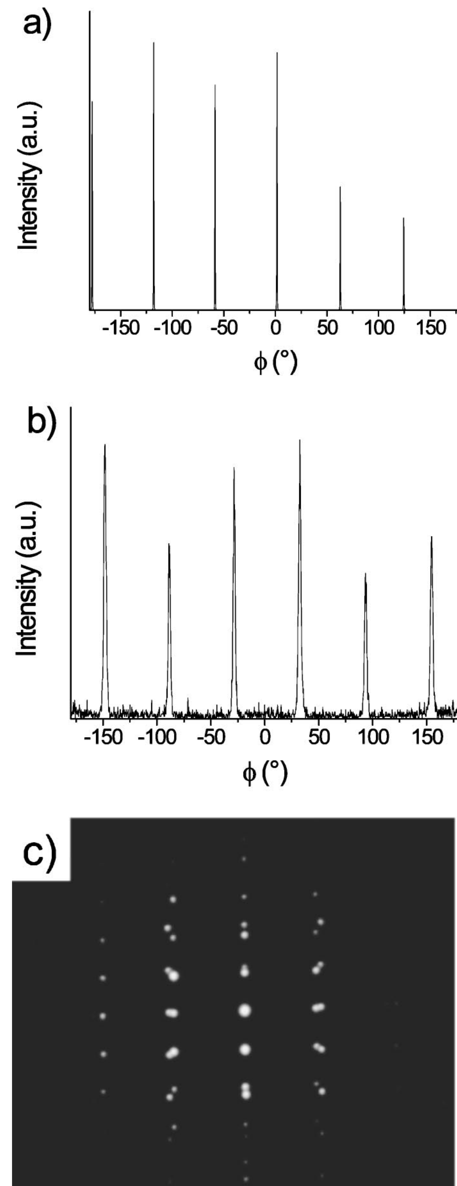

FIG. 4. (a) GaN{$\bar{1}$012} and (b) $LiNbO_3$ φ-scans and (c) electron diffraction pattern demonstrating epitaxial relationship between $LiNbO_3$ and GaN (incident beam along GaN[11$\bar{2}$0]). The $LiNbO_3$ has two rotational variants separated by 60° and a 30° in-plane rotation from the GaN.

The in-plane texture of the $LiNbO_3$ film on GaN was investigated by an x-ray φ-scan. The GaN {$\bar{1}$012} and $LiNbO_3${20$\bar{2}$4} φ-scans shown in Figs. 4(a) and 4(b), respectively, and the electron diffraction pattern (incident beam direction=GaN[11$\bar{2}$0]) shown in Fig. 4(c) indicate that the film grew epitaxially on GaN with crystallo-

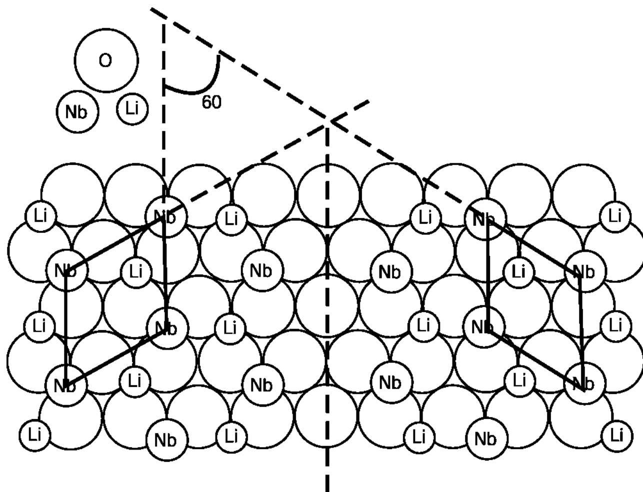

FIG. 5. Schematic showing two possible variants of $LiNbO_3$. After Derouin *et al.* (Ref. 15).

graphic registry. The $LiNbO_3$ *c*-plane was parallel to the *c*-plane of the GaN, but there was a 30° in-plane rotation between the two and the $LiNbO_3$ films had two variants of grains rotated 60° in-plane to each other. The in-plane relationship of the respective variants was $[1\bar{1}00]_{LiNbO_3} \| [11\bar{2}0]_{GaN}$ and $[10\bar{1}0]_{LiNbO_3} \| [\bar{1}2\bar{1}0]$GaN. The close-packed anion lattices of the $LiNbO_3$ and GaN have registry and a 60° rotational variant results in an identical anion packing and thus a continuous anion lattice. Therefore the difference between the two rotations is due to the cation positions. A similar structure has been observed on epitaxial $LiNbO_3$ on Al_2O_3.[15] The number of variants doubles when the orientation of the *c*-axis [i.e., (0001) or $(000\bar{1})$ orientation] is included. Only two of these variants are distinguishable in XRD patterns.[15] An example of a 60° rotational variant is shown in Fig. 5.

Figure 6(a) is an atomic force microscopy (AFM) image of the $LiNbO_3$ film on GaN, while Fig. 6(b) is an AFM image of $LiNbO_3$ on AlGaN/GaN. Outgrowths are evident in both images. Many more outgrowths are present on the $LiNbO_3$/AlGaN/GaN structure. It has been reported that outgrowths on $LiNbO_3$ films on (0001)-sapphire substrates are grains with polarization reversal (*c*-grains) that reduce the electrostatic energy of the film.[14] However, since GaN and AlGaN are polar materials while sapphire is not, the polar nature of the GaN and AlGaN/GaN surface could affect the growth of the $LiNbO_3$ films. In fact, it was assumed that the spontaneous polarization of the GaN and AlGaN would affect the growth of the $LiNbO_3$, and particularly the direction of the spontaneous polarization of the oxide.

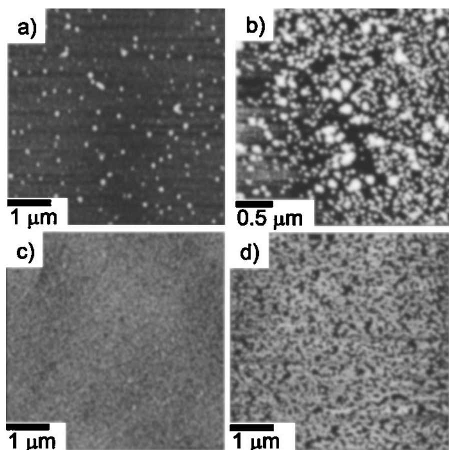

FIG. 6. (a) AFM image of $LiNbO_3$/GaN surface and (b) AFM image of $LiNbO_3$/AlGaN/GaN. Outgrowths are present on the $LiNbO_3$ films. (c) and (d) AFM images of $LiNbO_3$/GaN and $LiNbO_3$/AlGaN/GaN following etching in HF:HNO_3, respectively.

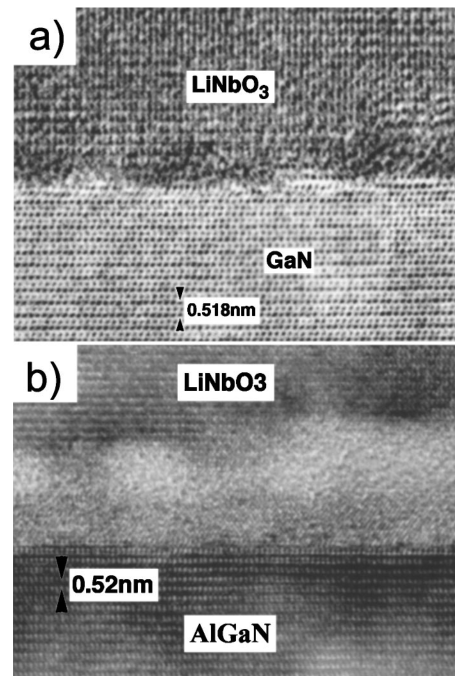

FIG. 7. High-resolution TEM images of the (a) $LiNbO_3$/GaN and (b) $LiNbO_3$/AlGaN interfaces.

The growth of *c*+ (that is, with the spontaneous polarization vector of the films pointing from the substrate to the surface of the films[14]) on sapphire has been reported for both sputter deposited[14] and MOCVD grown films.[16] It has been well established that the *c*− face of $LiNbO_3$ etches much faster in HF and HF:HNO_3 than the *c*+ face.[14,16,17] The outgrowths of sputter deposited $LiNbO_3$ films on sapphire were shown to be *c*− grains in a *c*+ matrix by etching in HF.[14] To investigate the polarity of our films, the samples were etched in HF:HNO_3 and investigated with AFM following etching. AFM images following etching are shown in Figs. 6(c) and 6(d). The pit density in the etched films corresponds to the density of outgrowths prior to etching the films. The result supports our proposal that the outgrowths are *c*− grains and the matrix of the film is *c*+. To further investigate the polarity of the films, CBED was performed on the films and will be further discussed below.

High-resolution cross-sectional TEM images of the $LiNbO_3$/GaN and $LiNbO_3$/AlGaN interfaces are shown in Fig. 7. A transition layer was observed at the interface be-

tween $LiNbO_3$ and GaN as well as in the $LiNbO_3$/AlGaN structure. From the diffraction pattern in Fig. 4(c), it can be seen that despite the observation of an amorphous layer, the $LiNbO_3$ films grew epitaxially on the GaN with the epitaxial relationship $[1\bar{1}00]_{LiNbO_3} \| [11\bar{2}0]_{GaN}$, confirming the relationship found by the x-ray φ-scans and possibly indicating that the amorphous layer was noncontinuous. The outgrowths were observed to be misaligned grains. The $LiNbO_3$ was completely removed from a $LiNbO_3$/AlGaN/GaN structure by etching in HF:HNO_3 and AFM was subsequently performed. The surface looked like a typical AlGaN surface, indicating that the transition layer was present completely in the $LiNbO_3$ layer and no interfacial reaction had occurred.

The crystal quality of the as-deposited $LiNbO_3$ was not high enough to perform CBED on the samples to confirm the polarization orientation. To improve the crystal quality, the $LiNbO_3$/GaN structures were annealed in N_2 at 900 °C for 1 min. XRD and TEM measurements showed that the crystal quality of the films was greatly improved by the anneal. The rocking curve FWHM was decreased from 0.92° prior to annealing to 0.36° following annealing. The transition layer at the interface was largely removed. Dark field TEM images showed that there were still some extended defects in the film and some amorphous regions that remained at the interface.

The improved crystal quality of the $LiNbO_3$ films made it possible to record CBED patterns. Further detail of the CBED experiments will be presented elsewhere.[18] As a separate determination of the film polarity, a series of CBED patterns were recorded at varying thicknesses. These images were compared to simulated CBED patterns. Companion samples of known polarity Ga-faced GaN films were also studied as a reference. Additionally, CBED patterns were taken of commercially available $LiNbO_3$ substrates of known polarity, both $c+$ and $c-$.

CBED images taken from the annealed $LiNbO_3$ film at different thicknesses as well as a $LiNbO_3$ substrate for reference and simulated images are shown in Fig. 8. The substrate patterns are shown in Fig. 8(a), while film thicknesses of 50 and 65 nm are shown in Figs. 8(b) and 8(c), respectively. The measured patterns are on the left and the simulated patterns are on the right. The simulated patterns closely match the experimental pattern for both the substrate of known polarity and the measured films, verifying the polarity determination of the films using this method. It was found that the postannealed $LiNbO_3$ films that were grown on GaN were in the $c+$ orientation, confirming the etching results discussed above. Again, this orientation is with the spontaneous polarization vector pointing from the substrate to the surface of the film,[14,19,20] which is opposite the orientation of the spontaneous polarization orientation in GaN and AlGaN/GaN structures grown by MOCVD (typically Ga-terminated).[7,8] It has been reported that homoepitaxial MOCVD grown $LiNbO_3$ films have a $c+$ orientation regardless of the polarity of the $LiNbO_3$ substrate.[16] To investigate whether or not the substrate polarity affected the $LiNbO_3$ film polarity, homoepitaxial $LiNbO_3$ films were sputtered on substrates with $c+$ and $c-$ orientations and CBED images were taken. The polarity of the films followed the polarity of the substrate, indicating that the orientation of the films was not an artifact of the deposition method.

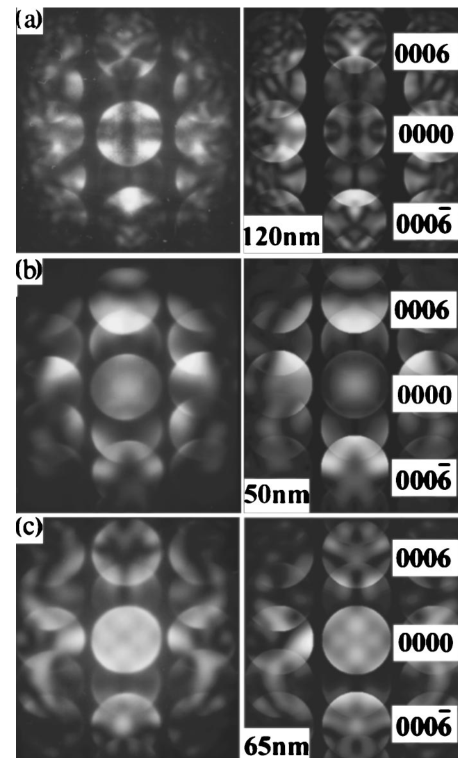

FIG. 8. Experimental (left) and simulated (right) CBED patterns of a $LiNbO_3$ substrate and annealed films of varying thickness showing perfect pattern match verifying polarity determination. The substrate pattern is shown in (a) and the film patterns are shown in (b) and (c).

For the materials system being considered, there are two competing effects that determine the orientation of the polarization in the $LiNbO_3$ crystal- the local ionic interactions of the first atomic layers with the underlying GaN (AlGaN) and the affinity of the film to follow the polarization direction of the substrate. A schematic of the $c+$ and $c-$ orientations of $LiNbO_3$ is shown in Fig. 9. In a $LiNbO_3$/GaN(AlGaN) structure, the first layer in the oxide will consist of oxygen atoms. The following stacking sequence of the cations will then determine the polarity of the film. In the $c+$ orientation, the Nb cations adjacent to the GaN are shifted above the center of the oxygen octahedra they are located in. In the $c-$ orientation, the Nb cations are shifted below the center of the oxygen octahedra and therefore closer to the Ga cations. It is possible that the $c+$ orientation is more energetically favorable than the $c-$ on a local scale than the $LiNbO_3$ film following the polarization of the underlying substrate due to the location of the Nb cation. The effects of the transition layer on the subsequent growth and orientation of the film is not currently understood.

Capacitors were formed on both AlGaN/GaN samples as well as n-GaN samples. The charge in the $LiNbO_3$/AlGaN/GaN structures was reduced by approximately 50% compared to the structure without $LiNbO_3$. The

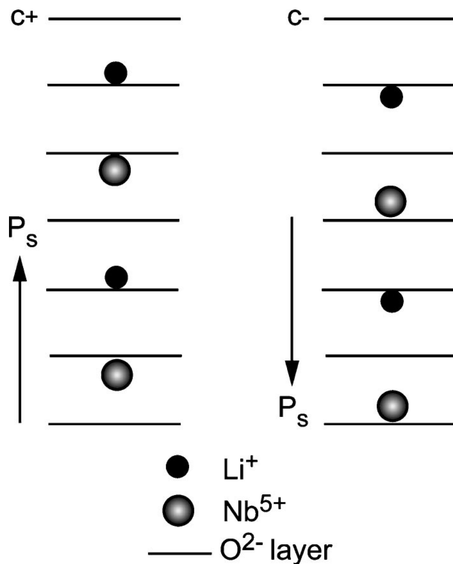

FIG. 9. Schematic of $LiNbO_3$ stacking sequence and corresponding spontaneous polarization vector for the $c+$ and $c-$ orientation.

near-surface charge was reduced in the n-GaN structures as demonstrated by differentiation of the capacitance–voltage ($C-V$) curves. We have recently shown that GaN-based structures are sensitive to the plasma used during rf-magnetron sputtering of thin oxide films,[21] and it is likely that at least some of the charge modification in the samples was due to damage. Postdeposition annealing under the same conditions used above resulted in recovery of the near-surface charge in the $LiNbO_3/n$-GaN structure, indicating that the reduction in charge was due to damage rather than polarization effects. There was no change in charge in the AlGaN/GaN structure following annealing. The magnitude of reduction in charge was larger than we have observed in other oxide/AlGaN/GaN structures, possibly indicating some polarization-induced effects in the charge. However, the growths performed here were also longer and at higher temperature than our previous growths, and both of these parameters seem to affect the amount of damage to the GaN during growth. Further analysis of electrical properties should be performed on structures grown using a nonenergetic growth technique so the effects of the deposition method can be removed from the results unambiguously.

IV. CONCLUSIONS

c-axis oriented $LiNbO_3$ thin films were epitaxially grown on (0001)-GaN templates and AlGaN/GaN structures using RF magnetron sputtering system. The $LiNbO_3$ films were shown to be single phase by XRD analysis. Off-axis x-ray phi-scans showed the existence of $LiNbO_3$ grains that were rotated by 30° in-plane to the GaN substrate and that the $LiNbO_3$ contained two variants of grains rotated 60° relative to each other. AFM images showed that the $LiNbO_3$ films had outgrowths. A transition layer was observed between $LiNbO_3$ film and GaN in the cross-sectional TEM image. Etching as well as CBED was used to verify the polarity of the $LiNbO_3$ films, and that the films grew with a spontaneous polarization vector opposite to that of the underlying GaN film.

ACKNOWLEDGMENTS

The authors would like to thank Marek Veithen for useful discussions. The authors would like to gratefully acknowledge support of the Office of Naval Research through the Center for Advanced Nitride Electronics (CANE), monitored by Dr. Harry Dietrich, and from DARPA under program manager Dr. Stuart Wolf. Sputtering system fabrication was supported by the Army Research Office (ARO) through DURIP equipment Award No. DAAD 19-99-1-0060. This work made use of MRL Central Facilities supported by the MRSEC program of the National Science Foundation under Award No. DMR00-80034.

[1]V. Gopalan, N. A. Sanford, J. A. Aust, K. Kitamura, and Y. Fujikawa, *Handbook of Advanced Electronic and Photonic Materials and Devices*, edited by H. S. Nalwa (Academic, New York, 2001), Vol. 4, p. 57.
[2]T. A. Rost, H. Lin, and T. A. Rabson, J. Appl. Phys. Lett. 59, 3654 (1991).
[3]K. Kim, IEEE Electron Device Lett. **19**, 204 (1998).
[4]M. Asif Kahn, J. N. Kuznia, D. T. Olson, W. J. Schaff, J. W. Burm, and M. S. Shur, Appl. Phys. Lett. **65**, 1121 (1994).
[5]H. Xing, S. Keller, Y. Wu, L. McCarthy, I. P. Smorchkova, D. Buttari, R. Coffie, D. S. Green, G. Parish, S. Heikman, L. Shen, N. Zhang, J. J. Xu, B. P. Keller, S. P. DenBaars, and U. K. Mishra, J. Phys.: Condens. Matter **13**, 7139 (2001).
[6]U. K. Mishra, Y. Wu, B. P. Keller, S. Keller, and S. P. DenBaars, IEEE Trans. Microwave Theory Tech. **46**, 756 (1998).
[7]O. Ambacher, J. Smart, J. R. Shearly, N. G. Weimann, K. Chu, M. Murphy, W. J. Schaff, L. F. Eastman, R. Dimitrov, L. Wittmer, M. Stutzmann, W. Rieger, and J. Hilsenbeck, J. Appl. Phys. **85**, 3222 (1999).
[8]I. P. Smorchkova, C. R. Elsass, J. P. Ibbetson, R. Vetury, B. Heying, P. Fini, E. Haus, S. P. DenBaars, J. S. Speck, and U. K. Mishra, J. Appl. Phys. **86**, 4520 (1999).
[9]Y. Lin, Y. Zhang, J. Singh, R. York, and U. Mishra, J. Appl. Phys. **89**, 1856 (2001).
[10]M. Singh, Y.-R. Wu, and J. Singh, Solid-State Electron. **47**, 2155 (2003).
[11]Y.-R. Wu, M. Singh, and J. Singh, J. Appl. Phys. **94**, 5826 (2003).
[12]M. Veithen and Ph. Ghosez, Phys. Rev. B **65**, 214302 (2002).
[13]W. A. Doolittle, G. Namkoong, A. Carver, W. Henderson, D. Jundt, and A. S. Brown, Mater. Res. Soc. Symp. Proc. **743**, 9 (2002).
[14]J. J. Kingston, D. K. Fork, F. Leplingard, and F. A. Ponce, Mater. Res. Soc. Symp. Proc. **341**, 289 (1994).
[15]T. A. Derouin, C. D. E. Lakeman, X. H. Wu, J. S. Speck, and F. F. Lange, J. Mater. Res. **12**, 1391 (1997).
[16]R. Hiskes, S. A. Dicarolis, J. Fouquet, Z. Lu, R. S. Feigelson, R. K. Route, F. Leplingard, and C. M. Foster, Mater. Res. Soc. Symp. Proc. **335**, 299 (1994).
[17]K. Nassau, H. J. Levenstein, and G. M. Loiacono, J. Phys. Chem. Solids **27**, 997 (1966).
[18]Y. Wu, P. J. Hansen, L. Shen, R. A. York, U. K. Mishra, and J. S. Speck (unpublished).
[19]S. C. Abrahams, H. J. Levenstein, and J. M. Reddy, J. Phys. Chem. Solids **27**, 1019 (1966).
[20]M. Veithen (private communication, 2004).
[21]P. J. Hansen, L. Shen, Y. Wu, A. Stonas, Y. Terao, S. Heikman, D. Buttari, T. R. Taylor, S. P. DenBaars, U. K. Mishra, R. A. York, and J. S. Speck, J. Vac. Sci. Technol. B **22**, 2479 (2004).